J. Fluid Mech. (1971), *vol.* 49, *part* 4, *pp.* 635–655
Printed in Great Britain

An experimental investigation of turbulent stratified shearing flow

By MICHAEL J. MOORE
AND ROBERT R. LONG
Department of Mechanics, The Johns Hopkins University

(Received 19 October 1970 and in revised form 8 April 1971)

Some experiments are described in which steady-state shearing flows are developed in stratified brine solutions contained in a cyclically continuous tank of rectangular cross-section. Over the range of overall Richardson numbers studied, the results suggest that whenever turbulent layers are present on either side of a region of fluid with a gravitationally stable density gradient, they cause erosion of this region to occur. The erosion leads to the formation of two homogeneous layers separated by a thin layer of strong density and velocity gradients. The gradient Richardson number, computed by using the velocity and density gradients in this transition layer, tends to have a value of order one.

If we define an overall Richardson number Ri^* by averaging the velocity and density gradients over the entire depth of fluid in the tank, we find that the non-dimensional buoyancy flux, Q, is functionally related to Ri^* by an equation of the form $Q = C_1(Ri^*)^{-1}$ where C_1 is a constant, approximately, and Ri^* ranges in value between one and thirty.

To check the effect of a large variation of the molecular diffusivity coefficient on flow conditions, we ran a limited number of experiments with thermally stratified fluid. Over a restricted range, $1{\cdot}0 \leqslant Ri^* < 5{\cdot}0$, velocity profiles very similar to those measured in the brine-stratified experiments at like values of Ri^* were obtained. This suggests that the coefficient of molecular diffusion is not an important parameter in either type of experiment.

Other experiments, made in the same apparatus, describe the entrainment by a turbulent, homogeneous layer of an initially quiescent layer of fluid with a linear density gradient. The depth of the turbulent layer, D, increases with time, t, according to the relation.

$$D^3 \propto t.$$

This result is consistent with that found by Kato & Phillips (1969), although the turbulent layer in the present experiment is generated in a different manner.

1. Introduction

The experiments described below were carried out to study some of the properties of turbulent shear flow in stratified systems like the oceans and atmosphere. There is evidence that both of these systems exhibit a layered structure (see, for example, the paper by Woods (1968) and the summary by Cooper (1967)

for the oceans, and the work of Ludlam (1967), Axford (1968), and Reiter (1969, p. 7) for the atmosphere). The density field of the ocean often consists of a succession of more or less homogeneous layers separated by sharp gravitationally stable interfaces. In the atmosphere, somewhat similar interfaces known as 'inversions' frequently occur. They are characterized by sharp changes in the potential temperature (or potential density) gradient and are more stable than the relatively thicker regions of fluid on either side of them. In both the oceans and atmosphere these thin gravitationally stable layers are often associated with high velocity gradients.

In discussing these geophysical systems, the non-dimensional parameter normally used is the gradient Richardson number, Ri, calculated at a given level in terms of the local mean density and velocity gradients. It is defined by

$$Ri = \left(\frac{\partial\overline{\rho}}{\partial z}\right) \Big/ \left(\frac{\partial\overline{u}}{\partial z}\right)^2, \tag{1}$$

where the *buoyancy* ρ is related to the density ρ_1 and a reference density ρ_0 by

$$\rho = g\left(\frac{\rho_1 - \rho_0}{\rho_0}\right). \tag{2}$$

In (1), $\overline{\rho}$ and $\overline{u}$ are the mean buoyancy and the mean horizontal velocity at the level z. We also use an overall Richardson number, Ri^*, calculated for a whole layer of fluid in terms of the density and velocity gradients averaged over the layer. It is defined by

$$Ri^* = H\Delta\rho/(2\Delta u)^2, \tag{3}$$

where H is the layer depth and $-\frac{1}{2}\Delta\rho$, $\frac{1}{2}\Delta\rho$ and Δu, $-\Delta u$ are the buoyancies and the velocities at the top and bottom of the layer in a co-ordinate system in which the top and bottom speeds are opposite in sign and equal in magnitude.

High shears associated with the thin stable layers mentioned above frequently result in a value of the Richardson number for the layer close to one. Woods (1968), for example, describes the occurrence of such layers in the ocean, while in the atmosphere, layers over which Ri has a value of order one are often associated with regions of clear-air turbulence. (See Ludlum or Axford or Reiter, cited above.)

Among the several experimental papers on stratified fluids in the literature are a number of useful ones concerned with the vertical transport of buoyancy and horizontal momentum across density jumps. These experiments are either horizontally inhomogeneous flows or non-steady shearing flows, or are characterized by the lack of a mean velocity. Later we will discuss and compare these with the present experiment in which steady-state horizontally homogeneous stratified shearing flows are achieved.

The simplest possible idealized experiment incorporating shear and stratification is one with turbulent liquid between two plates a distance H apart. The plates are moved in opposite directions along the x axis to produce a shear, and the density at each plate is fixed to create a stable vertical density distribution. The parameters of the problem are $\nu, K, H, \Delta u$ and $\Delta\rho$, where $-\Delta u$ and Δu are

the speeds of the lower and upper plates along the x axis, ν and K are the kinematic viscosity and kinematic diffusivity, and the fluid at the upper and lower plates is maintained at buoyancies of $-\frac{1}{2}\Delta\rho$ and $\frac{1}{2}\Delta\rho$.

If primes denote perturbations, the quantities

$$\tau = \nu\bar{u}_z - \overline{u'w'} \tag{4}$$

and

$$q = K\bar{\rho}_z - \overline{w'\rho'} \tag{5}$$

are the vertical fluxes of horizontal momentum and buoyancy. If the motion is statistically steady and if mean quantities do not vary horizontally, τ and q are constant in time and space. In turbulent flow in which ν and K are arbitrarily small, it may be assumed that the molecular fluxes can be neglected. If we then take $H, \Delta u$ and $\Delta\rho$ as relevant parameters of the experiment, the number Ri^* should be the non-dimensional number governing similarity between two given experiments.

The experiments in our apparatus consist of an entrainment type and a two-layer type and will be described in detail below. At this point, we note that the two-layer type of experiment reproduces the essential features of the idealized experiment described above, although the shear is generated by a different method.

2. The apparatus

The apparatus consists of a cyclically continuous tank with a system of slits and holes in the floor and ceiling, which enables fluid to be injected and withdrawn in such a manner that steady-state horizontally homogeneous shearing flows are generated. The cyclically continuous tank, referred to as the flow tank, is constructed of half-inch transparent Plexiglas. Figures 1 and 2 show views of the system.

The flow tank has two straight sections 290 cm long joined by two semicircular annuli of mean radii $22\frac{1}{2}$ cm. Fluid can be injected into the bottom of the flow tank with an almost horizontal trajectory, at an angle of 5° to the horizontal, through 24 slits spaced 30 cm apart and extending across the full width of the floor of the tank. An equal volume of fluid is withdrawn through a number of holes of diameter 5 mm in the floor to yield a zero mean vertical velocity at this plane.

A similar system of slits and holes in the ceiling of the flow tank allows the injection and withdrawal of fluid in a like manner, but the injection direction is opposite to that of the floor slits.

The injection and withdrawal of fluid at the bottom and at the top of the tank is accomplished by separate centrifugal pumps. Saline water is recirculated between the bottom section of the flow tank and a storage tank. Fresh water at room temperature is pumped from another storage tank through the top section of the tank and then to waste. The injection pipe system is designed to give, as accurately as possible, an equal volume-flow rate through each slit regardless of the magnitude of the total volume-flow rate.

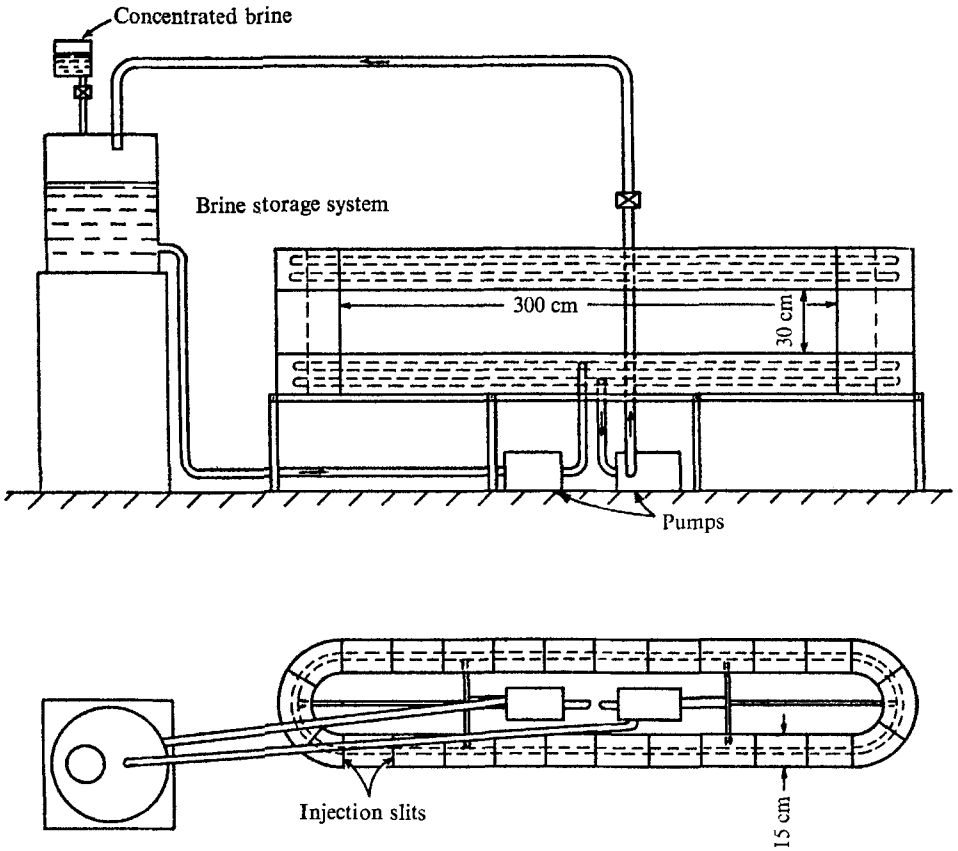

FIGURE 1. Overall diagram of experimental tank showing salt-water circulation pipes. Fresh water is circulated through the upper section of the tank in a similar manner. See figure 2 for details of injection-withdrawal system.

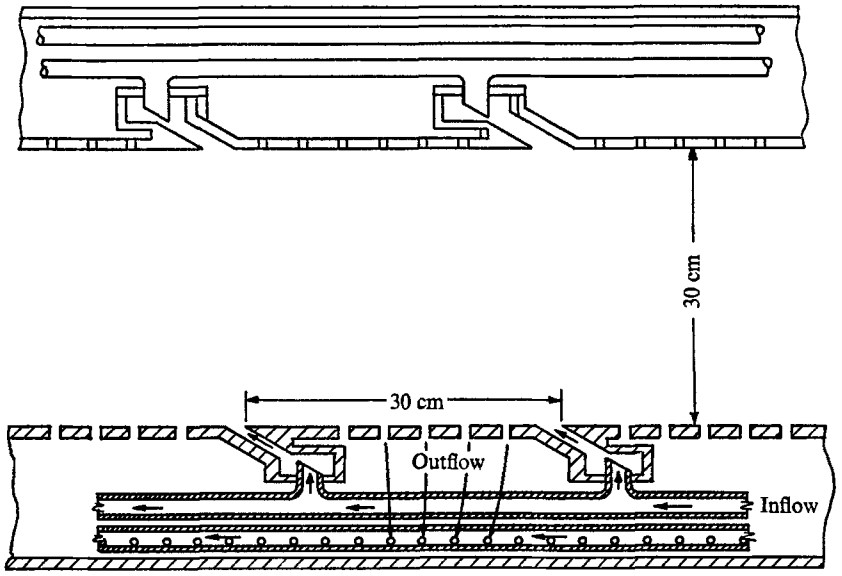

FIGURE 2. Sketch showing injection-withdrawal detail in both floor and ceiling of experimental tank.

As measured over the course of an experiment, the typical mean density profile has an inflexion point. One requirement for the desired steady-state condition is that the level of this inflexion point be kept constant in time. This is accomplished by adjusting the salt-water withdrawal rate to keep the level of the brine-storage system fixed.

In practice, the level of the storage tank is kept within 1 cm of the selected level. For 3 cm on either side of this selected level, the storage tank has a horizontal cross-sectional area equal to 0·06 of the horizontal cross-sectional area of the flow tank. The maximum variation of the level of the density inflexion point in the flow tank is thus kept at $\pm 0{\cdot}06$ cm. The upper surface of the flow tank is the 'perforated ceiling' (see figure 2) through which water is injected and withdrawn. Above this is the pipe withdrawal system just below the upper free surface of the water. The height of this surface is held constant.

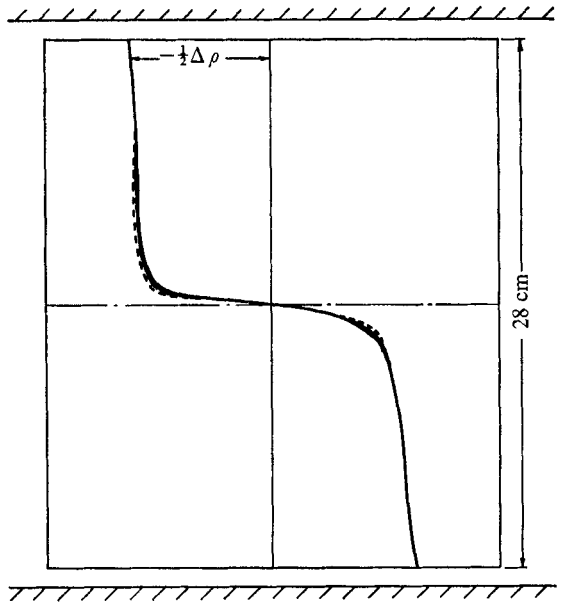

FIGURE 3. Density profiles along straight section of tank. —, profile at test section in middle of straight section of tank; – – –, profile near one end of tank.

One of the basic goals of the experiment was the horizontal homogeneity of the experimental flow. In achieving this, the problems caused by secondary motions resulting from the flow in the semi-annular ends had to be solved. To reduce the size of the eddies generated in these sections, and the excess mixing they produced, a number of combinations of vertical and horizontal partitions were tried. The best results were obtained using one vertical and one horizontal partition, dividing the cross-sectional area in the ends into four equal parts. With these and other adjustments, the slight effect caused by the excess mixing in the ends can be seen in figure 3.

The mean velocity profile is measured by using the hydrogen bubble technique (Clutter & Smith 1961). Platinum wire, stretched vertically in the tank, is used as the bubble generator, and the electrical pulses are produced at intervals of

one second or one-half second depending on the velocity of the fluid. The fluid 'time lines' marked by the bubbles are photographed by a camera located in front of the tank. The bubbles tend to rise slowly and this must be allowed for in evaluating the photographs. In a salt-stratified fluid, the lower portion of the wire, being in a more saline solution, conducts more current and gives off larger bubbles, so it was found necessary to split the wire into four segments, each being supported by insulated needles, and to vary the voltage applied to each segment to cause electrolysis.

The pulses are generated by a cam tripping an on–off switch. The cam shaft is driven by a variable speed motor, and the interval between trippings is found by timing the interval for twenty trippings. It is possible to set this for $20 \pm 0{\cdot}1$ sec (or $10 \pm 0{\cdot}1$ sec) so that the maximum time-error is 0·005 sec for the one-second pulses and 0·01 sec for the half-second pulses. The distance between 'time lines' can be read from the photographs to an accuracy of ± 2 mm. It is considered that the mean velocity measurements are in error by approximately 10 %. The velocities vary from 2 cm sec^{-1} to 6 cm sec^{-1} at the top and bottom of the tank, to zero velocity at the centre.

A hot-film anemometer was used to measure the r.m.s. turbulent velocity, $\tilde{u} = (\overline{u'^2})^{\frac{1}{2}}$, in some of the experiments. The set-up consisted of an anemometer in combination with a linearizer. The latter had a variable gain output so that the mean-voltage output could be made numerically equal to the mean velocity of the flow. The fluctuating voltage output was fed to a circuit which produced its root-mean-square value and this in turn was fed to a voltage integrator and integrated over a time period of up to 5 min. The measurement of the r.m.s. turbulent velocity at the midpoint of the homogeneous layers was carried out for mean velocities of 4·0, 4·5 and 5·0 cm sec^{-1}.

An electronic density probe is used to obtain mean density profiles. The probe itself is a single-point electrode conductivity device, and is essentially the same as that used by Odell & Kovasznay (1969). The response of the probe circuit to changes in salinity, and hence to changes in density, is almost exactly linear. Samples of the fluid are withdrawn from the top and bottom of the tank at periodic intervals and the density measured on a specific-gravity balance with an accuracy of 0·0001 g cm^{-3}. Thus, from a combination of the sampling and the conductivity probe, a good quantitative plot of the density profile is obtained. The density profiles are considered to have an accuracy of $\pm 2{\cdot}5$ %.

Over the length of time it takes to detect a quantitative change in the density of the saline water, namely 0·0001 g cm^{-3}, fluid in the salt-storage system circulates through the flow tank a number of times, and hence, any density change which is detected is considered to have occurred throughout the saline water in the pipes and storage system as well as in the flow tank itself.

3. Experimental procedure

3.1. *Two-layer type of experiment*

(i) *Brine-stratified experiments.* Initially, the whole circulation system is filled with fresh water. Salt water is then fed slowly into the bottom of the tank and fresh water taken out of the top until the tank is half-filled with brine solution. The level of the brine in the salt-storage system is set at this time. After some time, diffusion causes a more gradual density gradient to develop in the middle of the tank. The pumps are then started and the circulation of brine and fresh water commences.†

Probe traverses for the density profiles are normally made at 10 min intervals and samples taken every 15 min. From these two measurements, plus a knowledge of the total volume of salt water in the system (storage tank, pipes, and lower half of flow tank), the mass of salt lost over a 10 min period is estimated. Water is drawn out of the storage system continuously, salt is dissolved in it, and the concentrated brine is drip-fed back into the storage tank to maintain it at a fixed density and volume. The experiment is then run for an hour or more to check that the density and velocity profiles remain constant while salt is being added at this rate. This amount of salt passes through the flow tank from the bottom to the top and, when divided by the time and horizontal cross-sectional area of the flow tank, gives the salt-mass flux.

(ii) *Thermally stratified experiments.* The experimental procedure followed is similar to that for the brine-stratified solution. The cold water in the lower part of the flow tank is obtained by using commercial block ice to cool the required quantity of water. Block ice is also added to the storage tank (the 'brine-solution' storage tank of figure 1) in sufficient quantities to keep the temperature of the fluid circulating in this part of the system as constant as possible while an experiment is being run. A mixture of hot and cold tap water is fed into the 'fresh water' storage tank at the necessary rates to get the desired temperature for the fluid pumped through the upper part of the flow tank. Since we do not obtain density profiles in these thermal experiments, we are limited to observation of the velocity profile. The object, of course, is to compare the velocity profiles in the salt-water experiments and in the thermally stratified experiments at the same value of Ri^* in order to detect any effects due to the very different molecular diffusivities.

3.2. *Entrainment experiments*

In these experiments the flow tank is first filled with fluid that has a linear density gradient. Then the circulation of *either* the fresh *or* the salt water is begun in a manner similar to that for the two-layer experiments. The alteration of the mean density profile is then observed as a function of time.

† In a few experiments, the injection-withdrawal procedure was begun with an initial linear distribution of density in the flow tank. The final steady state was the same for the two initial conditions.

4. Results of steady-state two-layer experiments

The results obtained from experiments in which horizontal uniformity and steady-state conditions were achieved are shown in table 1 and listed in order of increasing values of Ri^*. Typical density and velocity profiles are shown in figures 4 and 5. A pronounced feature of the observations at high values of Ri^* (figure 5) is the thickness, $h \simeq \frac{1}{2}H$, of the homogeneous layers on either side of the region with the strong density gradient.

Ri^*	q (cm^2 sec^{-3})	$2\,\Delta u$ (cm sec^{-2})	$\Delta\rho$ (cm sec^{-2})	$Q \times 10^3$	L (cm)	Ri_L^*	h (cm)	$\tilde{u}/\Delta u$
0·7	0·021	8·0	1·5	1·70	24	0·56	3	—
0·7	0·028	9·0	1·9	1·57	24	0·57	3	—
1·0	0·020	8·4	2·5	1·00	14	0·49	8	—
1·1	0·017	8·0	2·4	0·88	14	0·52	8	—
1·1	0·026	10·0	3·7	0·70	12	0·44	9	0·13
1·2	0·020	9·0	3·2	0·69	12	0·48	9	0·14
1·2	0·014	8·0	2·5	0·70	20	0·78	5	—
1·4	0·0082	6·5	2·0	0·65	16	0·76	7	—
2·2	0·026	10·0	7·2	0·36	11	0·79	9·5	0·13
3·3	0·027	10·0	11·0	0·24	7	0·77	11·5	—
4·0	0·020	9·0	10·7	0·21	7	0·93	11·5	—
5·4	0·015	8·0	11·5	0·16	6	1·10	12	—
5·5	0·026	10·0	18·5	0·14	6	1·10	12	—
6·6	0·0047	5·5	6·7	0·12	4	0·89	13	—
7·5	0·022	10·0	25·0	0·088	4	1·0	13	0·13
12·0	0·019	9·5	36·0	0·056	2	0·80	14	—
13·5	0·023	10·0	45·0	0·05	4	1·8	13	0·13
14·4	0·016	9·0	29·0	0·046	2	0·97	14	—
15·0	0·013	8·0	32·0	0·05	4	2·0	13	0·14
16·0	0·0084	7·0	26·0	0·046	3	1·6	13·5	—
19·7	0·013	8·0	42·0	0·040	2	1·3	14	—
25·6	0·016	8·5	61·6	0·031	2	1·7	14	—
30·0	0·0083	7·0	49·0	0·024	3	3·0	13·5	—
44·0	0·0090	7·0	72·0	0·015	2	3·0	14	—
61·5	0·0041	6·0	74·0	0·0092	2	4·1	14	—

TABLE 1. The overall Richardson number is $Ri^* = H\Delta\rho/(2\Delta u)^2$ where H is the 30 cm depth over which the mean velocity and density profiles are measured. q is the buoyancy flux; $\Delta\rho$ is the buoyancy difference between the top and bottom layers of fluid; Δu is the mean velocity of either of these layers; Q is the non-dimensional buoyancy flux, $q/\Delta\rho(2\Delta u)$; L is the distance over which the velocity gradient has a constant value; h is the depth of either homogeneous layer; Ri_L^* is the overall Richardson number scaled on height L; and $\tilde{u}/\Delta u$ is a measure of the turbulence level in a layer.

One of the original purposes of this experiment was to investigate the validity of a theory by Long (1970) in which turbulent shearing flow was presumed to exist at high values of Ri^*. The theory, however, assumed thin turbulent boundary layers compared with the total depth H. This, of course, is not satisfied by the experimental observations. It is still a question whether this is characteristic of this general type of experiment or whether it is caused by some peculiarity of the

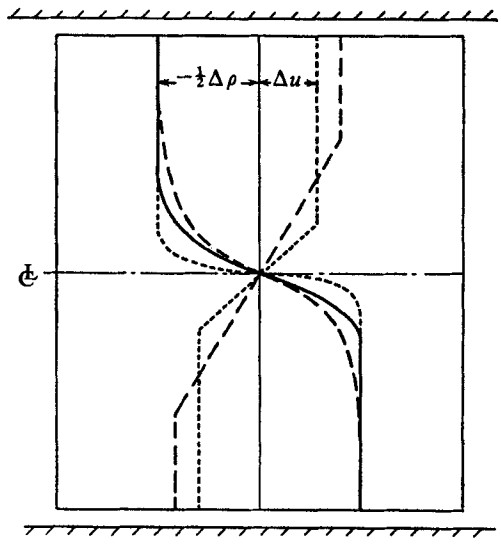

FIGURE 4

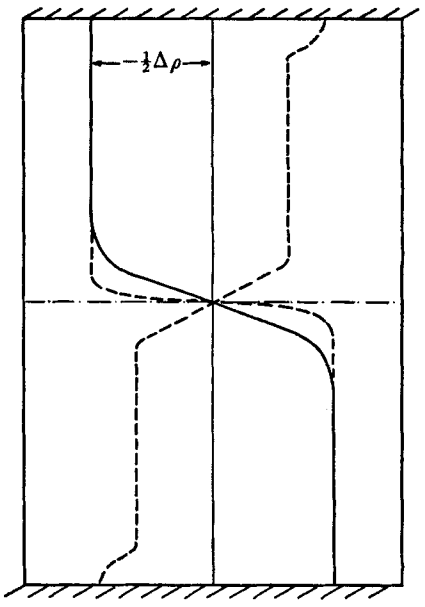

FIGURE 5

FIGURE 4. Mean velocity and mean buoyancy for two of the lower values of Ri^* with $\Delta\rho = 7{\cdot}2$ cm sec^{-2}.

Velocity and density	Δu cm sec^{-1}	Ri^*	q cm^2 sec^{-3}
—	0	—	—
· · · · ·	3·5	4·4	—
– –	5·0	2·2	0·026

FIGURE 5. Mean velocity and mean buoyancy for high value of Ri^*. The wall jets that occur in this experiment were caused by a modification in the apparatus which yielded a smaller injection angle for the slits.

Velocity and density	Δu cm sec^{-1}	Ri^*	q cm^2 sec^{-3}
—	0	—	—
– – –	4	15	0·013

apparatus. Initially we thought that any possible tendency for the formation of a gradual density gradient in the central section of the flow with thin turbulent boundary layers was eliminated by the large-size eddies which were present in the apparatus owing to the large angle at which fluid was injected. Modifications were made and this injection angle was reduced from 12° to 5°. This change, however, caused only slight differences in the velocity and density profiles except for the appearance of pronounced wall jets (figures 5 and 6, plate 1) next to the floor and ceiling in the second series of experiments. These jets were typically of the order of 2 cm thick, and their mean velocity was approximately one and one-half times that of the rest of the fluid in the homogeneous layer.

The development of the density and velocity profiles is best considered in relation to the various values of Ri^*. For values of Ri^* greater than approximately 3, the turbulence generated in each homogeneous layer is sufficient to erase to a considerable extent the region over which the density gradient was initially manifested. Two homogeneous layers separated by a region of very steep density gradient are produced, and the resulting interface is clearly visible as in figure 7 (plate 2). This surface is irregular in shape, and wisps of fluid are detached from the crests of the disturbances in a manner similar to that described by Rouse & Dodu (1955) and Kato & Phillips (1969). Figure 7 contains a sketch of a possible mechanism for the wisp detachment. The interface was normally covered with undular disturbances with an amplitude of the order of 0·5 cm, a wavelength of 3–4 cm and width of 1 cm. It is easier to see those which protruded from the interface into the top homogeneous layer than to see those protruding into the bottom layer, and occasionally the 'shadow' of a particular disturbance can be identified. These shadows are formed on the white background when collimated light is projected horizontally through the tank. The disturbances lie within the layer over which the velocity gradient is linear and move with a speed less than that of the homogeneous layer just above them. The disturbance and its shadow can be seen to grow in amplitude as the top of the undulation sharpens into a crest. Instead of breaking to form an eddy, however, the crest disappears suddenly. At this instant a long wisp 'shadow' appears to leave the location of the crest tip. From looking at motion pictures of this phenomenon, it seems likely that the original undular disturbance is caused by an eddy, from the homogeneous layer, 'scouring' the surface. The 'roller action' of this eddy then draws the more dense fluid up into a crest and the wisp appears as the crest sharpens and is then sheared off. The remainder of the disturbance then slowly subsides back into the region of maximum density gradient. This process apparently transfers most of the measured buoyancy flux in the range $3 < Ri^* < 30$. This flux is much greater than the molecular flux that is diffused through the region of maximum density gradient as shown in table 2.

As Ri^* decreases to the range $1{\cdot}5 < Ri^* < 3{\cdot}0$, the interface becomes more irregular and finally breaks down into a diffused region. The mean density change occurs over a greater depth of fluid than that corresponding to higher values of Ri^*, and the mean density profile begins to show curvature. The depth over which the velocity profile is linear increases as does the measured salt flux. The shadow patterns in figure 8 (plate 3) clearly show evidence that part of the mixing is now caused by internal wave breaking or roller formation.

Table 1 lists the distances, L, over which the velocity gradient is approximately linear. It is never greater than 24 cm, and for the lower values of Ri^*, the density profiles show that some variation in density occurs over most of this distance. For higher values of Ri^*, the density profiles show a vertical variation over smaller distances than L. As we have already indicated, the remaining distances, h, above and below this linear velocity gradient, are composed of more or less homogeneous fluid in turbulent motion. If an overall Richardson number is calculated using the average density gradient and the average velocity gradient over the length, L, it has a value close to one. The Richardson numbers based on this

length have been calculated for the various experiments and are shown in table 1 under Ri_L^*.

Three experiments were run at values of $Ri^* \geqslant 30$. The results are shown in tables 1 and 2. These flows were characterized by two factors which made them different from the other experiments: (i) Even though the values of L were very small, the density gradients over this L were so high that Ri_L^* had values $\geqslant 3{\cdot}0$. In contrast to this, we can note from the data that of the remaining experiments, only four have values of $Ri_L^* > 1{\cdot}3$ and none have values of $Ri_L^* > 2{\cdot}0$. (ii) Because of the very high values of these density gradients, the molecular fluxes were so large that they account for up to 34 % of the measured fluxes.

Ri^*	q (cm^2 sec^{-3})	$q \times 10^2$ (molecular) (cm^2 sec^{-3})	$\Delta q(\bar{\rho}) \times 10^2$ (cm^2 sec^{-3})	$\frac{\Sigma \Delta q}{q}$ (%)
0·7	0·021	Negligible	0·07	3·3
0·7	0·028	Negligible	0·05	1·8
1·0	0·020	Negligible	0·07	3·5
1·1	0·017	Negligible	0·07	3·7
1·1	0·026	Negligible	0·07	3·5
1·2	0·020	Negligible	0·07	3·5
1·2	0·014	0·004	0·1	7·2
1·4	0·0082	0·02	0·07	10·5
2·2	0·026	Negligible	0·09	2·7
3·3	0·027	Negligible	0·07	2·6
4·0	0·02	0·01	0·07	4·0
5·4	0·015	0·01	0·1	7·3
5·5	0·026	0·01	0·07	3·1
6·6	0·0047	0·01	0·02	6·4
7·5	0·022	0·02	0·07	4·5
12·0	0·019	0·03	0·11	7·8
13·5	0·023	0·03	0·11	6·1
14·4	0·016	0·03	0·1	8·1
15·0	0·013	0·02	0·08	9·2
16·0	0·0084	0·02	0·05	8·4
19·7	0·013	0·03	0·07	7·8
25·6	0·016	0·04	0·1	8·7
30·0	0·0083	0·04	0·05	10·8
44·0	0·009	0·1	0·08	20
61·5	0·0041	0·11	0·03	34

TABLE 2. Buoyancy fluxes in brine-stratified experiments. q is the measured flux; q (molecular) is the molecular diffusion flux occurring at the region with the highest density gradient measured in any particular experiment; $\Delta q(\bar{\rho})$ is the possible error in measuring q due to the uncertainty in the measurement of density. $\Sigma \Delta q/q$ is the percentage of the possible error in the measured flux. For a discussion of these errors, see the appendix.

Because of (i) and (ii) we feel that these experiments were not comparable to those with $Ri^* < 30$. In addition, although the experiments with $Ri^* > 30$ were run as long as 6 h, the measured fluxes were so small that the possible error in density measurement could appreciably affect their values.

Two experiments were made at values of $Ri^* < 1{\cdot}0$. In these flows, very large eddies (6–8 cm in diameter) extended through the diffused 'interface'. The

velocity fluctuations appeared to approach the order of the mean velocity (Δu) of the turbulent boundary layers and it was hard to obtain mean velocity profiles. Repeated traverses of the density probe were made to obtain mean density profiles.

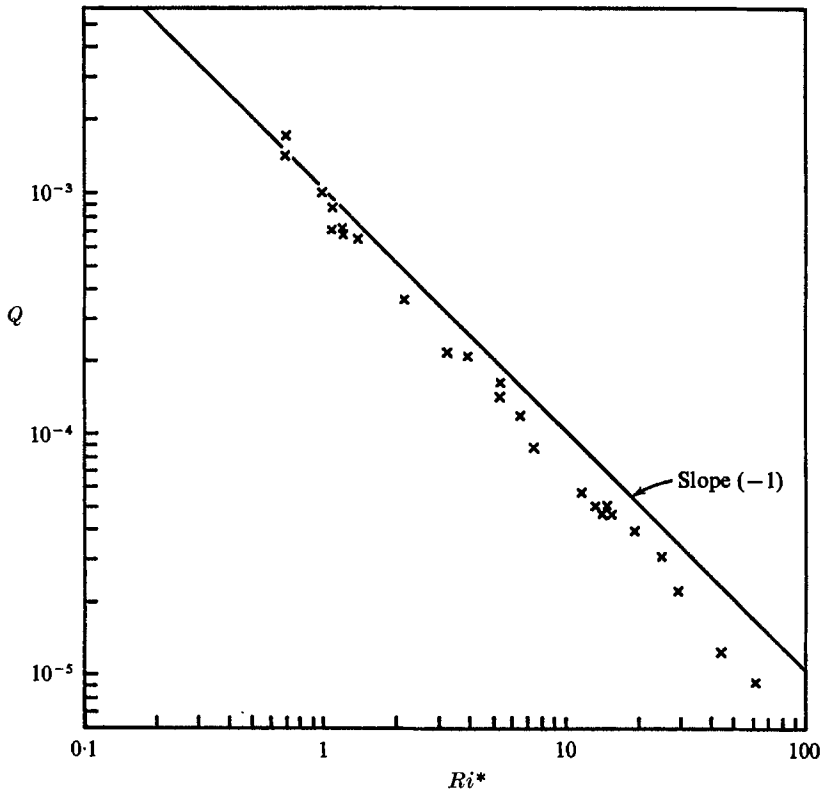

FIGURE 9. Plot of the non-dimensional buoyancy flux, Q, against the overall Richardson number, Ri^*.

We can consider the results of the two-layer experiments in which optimum flow conditions were achieved in the following manner: the Reynolds number, $\Delta uH/\nu$, varied from 8×10^3 to 15×10^3 and was not as high as desired. On the other hand, over the range $1 \leqslant Ri^* \leqslant 30$, the measured salt-flux was at least thirty times greater than that due to molecular effects; also, over the range, $1 \leqslant Ri^* < 5$, we found no significant differences between the velocity profiles of brine-stratified and thermally stratified shearing flows indicating that the molecular diffusitivity coefficient, K, is not an important parameter in this range. As a working hypothesis, we have therefore assumed the phenomena independent of ν and K. The pertinent constants of the experiment τ and q, should then be functions of $\Delta u, \Delta\rho$, and H. Thus, we get a non-dimensional buoyancy flux,

$$Q = q/2\Delta u \Delta\rho, \tag{6}$$

as a function of the overall Richardson number,

$$Ri^* = H\Delta\rho/(2\Delta u)^2. \tag{7}$$

Figure 9 shows Q plotted against Ri^* on log-log paper and a slope of (-1) is indicated for $1 \leqslant Ri^* \leqslant 30$. This implies a functional relation of the form

$$Q = C_1/Ri^*, \tag{8}$$

where C_1, which may have some dependence on ν and K, has a value of approximately 8×10^{-4} with an uncertainty of $\pm 20\,\%$.

It is instructive to compare the results given in this section with those from related experiments reported in the literature. Previous experiments have usually been studies of the rate of entrainment of a layer of fluid of one density by a turbulent layer of fluid of a different density. The entrainment velocity is defined as the normal velocity of the interface or, in the case of steady-state experiments, as the volume-flow rate of the fluid being entrained, divided by the cross-sectional area over which the entrainment is occurring. The entrainment rate, E, is then specified as the ratio of the entrainment velocity to some representative velocity for that particular experiment, and a functional relation is found from the data between E and the computed Richardson number for that particular experiment. As we shall see, this is comparable to a relationship between Q and Ri^*. As the Richardson numbers for these previous experiments frequently differ from our Ri^*, we shall note, wherever possible, the range of Ri^* over which these experiments were run. In all of the Richardson numbers defined below, $\Delta\rho_1$ represents the density jump between the homogeneous turbulent layer and the main body of the fluid being entrained. B_i is a constant for any particular experiment, the different experiments being denoted by different values of the subscript i.

Rouse & Dodu (1955) studied the rate of entrainment that occurs across an interface between two superimposed layers of fluid of slightly different densities when they generated turbulence in the upper layer using a mechanical agitator. They were the first to point out that if the entrainment rate is inversely proportional to the first power of the Richardson number, this implies that the rate of change of potential energy due to the entrainment process is proportional to the rate of production of turbulent energy by the stirring action of the agitator. Their own experiments (using salt) did not verify this relationship.

Ellison & Turner (1959) studied the flow of a layer of heavy saline solution down a sloping bottom under a deep layer of fresh water at rest. Their overall Richardson number, Ri^*_{hE}, was defined by

$$Ri^*_{hE} = \frac{g\Delta\rho_1}{\rho_0}\frac{D}{\overline{u}^2}, \tag{9}$$

where D is the entrained depth of fluid and $\overline{u}$ is its mean velocity. For a range of $Ri^*_{hE} \leqslant 1$, their results are consistent with a relation of the form,

$$E = B_E/Ri^*_{hE}, \tag{10}$$

where variations of Ri^*_{hE} are measured spacially along the bottom.

Lofquist (1960) investigated a layer of salt water flowing horizontally under still fresh water. His Richardson number is defined by

$$Ri^*_Q = (g\Delta\rho_1/\rho_0)h_1/\overline{u}^2, \tag{11}$$

where h_1 is the depth below the density inflexion point, and $\bar{u}$ is the mean velocity of the saline layer. It is thus essentially equal to $2Ri^*$. For values of $Ri_Q^* < 1{\cdot}0$ his data is consistent with

$$E = B_Q/Ri_Q^*. \tag{12}$$

For values of $Ri_Q^* > 1$, his data is very scattered but the entrainment rate appears to decrease at a faster rate than is given by (12).

Turner (1968) studied mixing rates across a density interface. He used both salt-stratified and thermally stratified fluids in order to investigate the effect of a change in the molecular diffusivity on the mixing rates. Turbulence was generated on either one side or both sides of the density interface by a mechanical stirrer, actually a rectangular array of bars forming a grid. The Richardson number used,

$$Ri_n^* = \frac{g\Delta\rho_1}{\rho_0}\frac{1}{ln^2} \tag{13}$$

(where n is the frequency of the stirrer and l is a length scale representative of the length of the energy-containing turbulent eddies, taken to be the distance between the bars of his stirring grid) is a type of overall Richardson number. For values of $Ri_n^* < 1{\cdot}0$, his entrainment rates for both brine-stratified and thermally stratified fluid appear to obey the law

$$E = B_n/Ri_n^*. \tag{14}$$

For values of Ri_n^* greater than one, he found that a relation of the same form as (14) was valid for the entrainment rate of thermally stratified fluid but that the entrainment rate for brine-stratified fluid decreased to

$$E = B_n/(Ri_n^*)^{\frac{3}{2}}. \tag{15}$$

He considered this reduced rate to result from the fact that the molecular diffusivity of salt is lower than that of heat.

Kato & Phillips (1969) studied the rate of entrainment of an initially linearly stratified fluid when the entraining fluid is a homogeneous turbulent layer generated by a constant stress, τ, applied to the upper surface. Using the friction velocity, $u_* = \tau^{\frac{1}{2}}$, as their scale velocity and the depth of the homogeneous layer as their scaling length, they found a result of the form

$$E = B_D/Ri_D^*, \tag{16}$$

where

$$Ri_D^* = g\Delta\rho_1 D/\rho_0 u_*^2. \tag{17}$$

D is the depth of the homogeneous layer and $\Delta\rho_1$ is the density jump at the interface between the homogeneous layer and the linearly stratified layer. As such, their Ri_D^* is a type of overall Richardson number and their range of values for Ri_D^* was equivalent to a range of values of $Ri^* < 1$.

In summary, a relationship of the form

$$E = B_p/Ri_p^*, \tag{18}$$

where Ri_p^* represents an overall Richardson number for that particular experiment and B_p a particular constant for that same experiment, appears to be valid for a wide variety of experiments when the stratified-fluid flow conditions are such that the values of Ri^* are $\leqslant 1$.

For those experiments which have the relation (18) between the particular Richardson number for that experiment and the entrainment rate, E, this rate represents, in non-dimensional terms, a time rate of change of potential energy per unit mass V_1 (Kato & Phillips 1969). Their result is

$$\frac{2\rho_0}{\Delta\rho_1 g u_*}\frac{dV_1}{dt} = \frac{u_e}{u_*} = E = \frac{B_D}{Ri_D^*}. \tag{19}$$

We may use the relationship between E and rate of change of potential energy to find a basis for comparing these entrainment experiments with our two-layer type of experiment in the following manner. The buoyancy flux, q, has the dimensions of time rate of change of energy per unit mass, and, when non-dimensionalized to the flux, Q, is functionally related to Ri^* by (8), and this is similar to the relation between E and Ri_D^* in (19). We calculate q by computing the vertical mass-flow rate per unit area from the quantity of salt added and then converting this to the buoyancy flux. Let dm be the mass that has passed from the bottom to the top of the tank in time dt. Since the mass is lifted a distance H, we call $gHdm$ the increment in potential energy, dV, due to this mass transfer. Thus

$$dV/dt = (dm/dt)gH. \tag{20}$$

If we average the rate of increase of potential energy over the mass of fluid in the flow tank, we obtain

$$\frac{dV_1}{dt} = \frac{1}{\rho_0 HA}\frac{dV}{dt} = \frac{1}{A}\frac{dm}{dt}\frac{g}{\rho_0}. \tag{21}$$

The term on the right is the buoyancy flux since it represents the vertical mass flux as measured experimentally, $A^{-1}\,dm/dt$, converted to the buoyancy flux by multiplying by g/ρ_0. Equation (21), therefore, is

$$dV_1/dt = q. \tag{22}$$

Thus, (22) indicates, in the sense in which we have discussed the process here, that q can be thought of as a time rate of change of potential energy per unit mass of the fluid experiencing the shear flow. If we non-dimensionalize it we obtain

$$(1/2\Delta u\,\Delta\rho)\,dV_1/dt = Q = C_1/Ri^*. \tag{23}$$

Comparing this with (19) it is evident that Q and E represent similar quantities and they are related to overall Richardson numbers in the same functional way.

We may derive this relationship between Q and E more directly. Thus, as we have seen,

$$q = \overline{w'\rho'} = (g/\rho_0 A)\,dm/dt. \tag{24}$$

The interface is fixed in a steady state, but we may alter the experiment to obtain a rising interface by turning off the injection-withdrawal system at the top. The interface then rises a distance $dh = u_e dt$. In the flow tank, we have

$$\text{mass}(t+dt) - \text{mass}(t) = \text{mass added at bottom} = dm.$$

If the lower density of $\rho_1 + \frac{1}{2}\Delta\rho_1$ and the upper density is $\rho_1 - \frac{1}{2}\Delta\rho_1$, we have

$$(\rho_1 + \tfrac{1}{2}\Delta\rho_1) A(\tfrac{1}{2}H + dh) + (\rho_1 - \tfrac{1}{2}\Delta\rho_1) A(\tfrac{1}{2}H - dh)$$
$$- (\rho_1 + \tfrac{1}{2}\Delta\rho_1)\tfrac{1}{2}AH - (\rho_1 - \tfrac{1}{2}\Delta\rho_1)\tfrac{1}{2}AH = dm,$$

or
$$u_e = (1/\Delta\rho_1 A)\, dm/dt, \tag{25}$$

or
$$u_e \Delta\rho = q. \tag{26}$$

Returning to the steady-state experiment, we now define u_e by this equation. With this definition Q and E are proportional to each other.

The present experiment thus indicates that we can extend the range of Richardson numbers over which (18) is valid from $0 \leqslant Ri^* \leqslant 1$ to $0 \leqslant Ri^* \leqslant 30$ provided the entrainment is occurring in a shearing flow. This result differs from that indicated by Lofquist's data and that obtained by Turner. In Lofquist's case the difference may stem from the horizontal inhomogeneity of his experiment. In Turner's case, it may be due to (i) the absence of a mean velocity in his flow, (ii) his method of defining the Richardson number, or (iii) what he calls the absence of the fine structure of turbulence from his experiments. He describes (iii) as a property associated with the low Reynolds numbers of his experiments. One difference between the entrainment procedure described by Turner and the one observed in the present experiments is the shearing off of the crests of the disturbances as they move into the region of increasing mean velocity. (This is the effect due to (i) above.) In contrast we can note that he attributes the slower mixing rates for salt (when compared to those for heat) at values of $Ri_n^* < 1$, "to the slower rate of incorporation of an entrained element (i.e. a disturbance) into its surroundings by diffusion which increases the tendency for it to return to the interface and to dissipate energy in wave-like motions". In our experiment the top part of such a disturbance would be sheared off thus indicating the presence of more of the 'fine structure' of the turbulence in our flow than in his.

It is difficult to compare the range of values of Ri_n^* with Ri^*, but, since Turner found the relationship (18) valid for thermally stratified flows with $Ri_n^* > 1{\cdot}0$, we ran three thermally stratified experiments with our apparatus to see if any differences in the flow pattern could be detected. We could detect no significant difference between the velocity profiles in either brine-stratified or thermally stratified shear flows with the same value of Ri^*. Assuming that the density profiles were also similar in both types of flow, we may conclude that (8) is valid for the range of Ri^* which the experiments covered, namely,

$$1{\cdot}0 < Ri^* < 5{\cdot}0.$$

These results suggest that over this small range of Ri^*, a large variation in the coefficient of molecular diffusion, K, produces no significant differences in the velocity profiles and hence at least partially supports the assumption that K is not an important parameter in our experiment.

The above relationships can be considered in terms of energy changes. Kato & Phillips showed in their experiments that the rate of increase of potential energy per unit mass is related to the rate of turbulent energy dissipation per unit mass in the turbulent shear layer. From (17) and (19) we have

$$dV_1/dt = \tfrac{1}{2}B_D u_*^3/D. \tag{27}$$

Batchelor (1953) states that it is found experimentally that the rate of change of turbulent kinetic energy per unit volume in isotropic turbulence is given by

$$\epsilon = d\tilde{u}^2/dt \simeq \tilde{u}^3/l_1, \tag{28}$$

where ϵ is the turbulent energy dissipation rate and l_1 is the diameter of the energy containing eddies. Townsend (1958) uses (28) for shear flows in a stably-stratified atmosphere in which the direct effects of buoyancy on the motion are small. On the assumption that this is applicable in an entrainment experiment, that the friction velocity $u_* \simeq \tilde{u}$, (Townsend 1956) and that the homogeneous layer depth, D, is of the order of the size of the energy containing eddies, then

$$\epsilon \simeq u_*^3/D. \tag{29}$$

Thus
$$dV_1/dt \simeq u_*^3/D \simeq \epsilon. \tag{30}$$

This relationship is the result quoted by Kato & Phillips. A similar one is given by Turner (1968) and by Long (1970). In the present experiment

$$q/\Delta\rho(2\Delta u) = C_1(2\Delta u)^2/H\Delta\rho \tag{31}$$

and thus using (22)

$$dV_1/dt = q = 8C_1(\Delta u)^3/H. \tag{32}$$

Equation (32) is not in the form (30); however, from the measurements which were made of $\tilde{u}$ as Δu varied over the range 4–5 cm sec^{-1}, a relation of the form

$$\tilde{u} \simeq C_2(\Delta u) \tag{33}$$

is evident. Here C_2 is a constant with a value of approximately 0·13.

If we assume (33) is valid for all Δu in our experiments then (32) is equivalent to (30). The experimental results, including our own, thus suggest that in geophysical flows and laboratory experiments of our type

$$dV_1/dt \text{ (or } q) \propto \epsilon. \tag{34}$$

The 'constant' of proportionality may, however, vary with μ and K although this seems unlikely in geophysical flows. Further experimentation would be desirable to investigate the possible variation of the 'constant' with these molecular quantities.

5. Results of the entrainment experiments

Our entrainment experiments indicate that an initially linear density gradient in the tank is eroded and replaced with a growing homogeneous layer of depth $D(t)$ when the injection-withdrawal is applied either at the bottom or the top of the channel. The results are shown in figure 10 as a plot (on log-log paper) of the entrainment depth versus time. The linearity of the graphs is consistent with $D^3 \propto t$ as was also found by Kato & Phillips (1969) although the shear was caused by different mechanisms in the two experiments. Their experiments were carried out for conditions which were equivalent to $Ri^* < 1$; the present ones have $Ri^* > 1$.

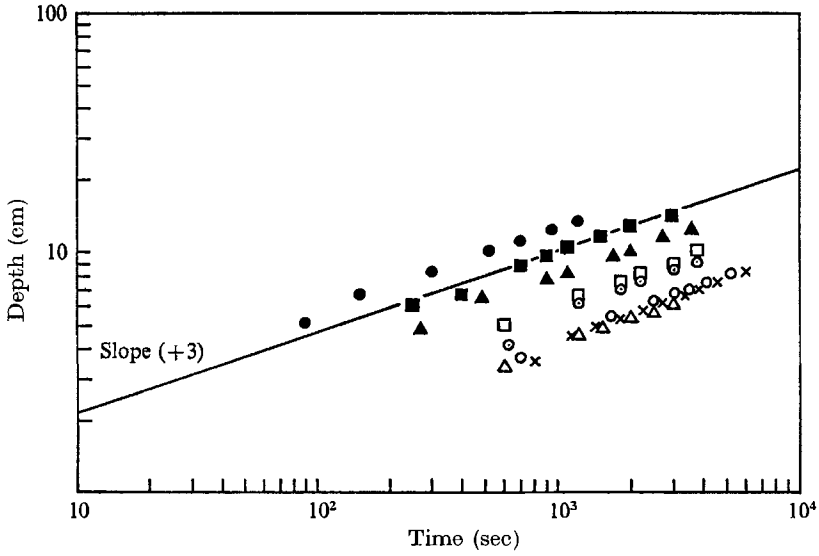

FIGURE 10. Plot of the entrained depth of homogeneous fluid against time in the entrainment experiments. N_0 is the initial Brunt–Väisälä frequency.

N_0	Symbol	Δu (cm sec^{-1})	Symbol	Δu (cm sec^{-1})
0·66	×	4·0	⊗	5·0
0·33	▲	3·0	■	3·5
0·30	△	2·2	□	1·5
0·50	○	2·0	⊙	2·5

The research reported in this paper was supported in part by the U.S. Department of Commerce, Environmental Science Services Administration under grant no. E22-36-70(G)

Appendix. Errors in the buoyancy flux

If the experiment is horizontally homogeneous, any net change with time in the mean density profile in a region results from the convergence of the vertical mass flux into or out of that region or from the occurrence of a mean vertical velocity. The unsteadiness is eliminated by the controls used in the experiment except that the density can only be determined to within 0·0001 g cm^{-3}. Also, the addition of the salt mass to the salt-water storage system, while keeping the fluid level in it constant, adds a small volume to the bottom of the experimental tank and hence causes a small positive vertical velocity at all levels. These two unwanted effects may be discussed by considering the continuity equation,

$$\partial\rho_1/\partial t + \nabla.(\rho_1\mathbf{u}) = 0. \tag{A 1}$$

Let
$$\rho_1(\mathbf{x},t) = \bar{\rho}_1(z,t) + \rho_1'(\mathbf{x},t) \tag{A 2}$$

and
$$\mathbf{u}(\mathbf{x},t) = \bar{\mathbf{u}}(z,t) + \mathbf{u}'(\mathbf{x},t), \tag{A 3}$$

where the bar denotes an average obtained by integrating over the horizontal area of the experimental tank at height z.

Substituting (A 2) and (A 3) into (A 1) and integrating over a volume of the experimental tank of cross-sectional area A and height z, we get

$$\frac{\partial}{\partial t}\int_0^z \bar{\rho}_1(z,t)\,dz + \bar{\rho}_1\,\overline{w}\Big|_0^z + \overline{\rho_1' w'}\Big|_0^z = 0. \tag{A 4}$$

Ideally we would like to consider that almost all of the measured salt flux comes from $\overline{\rho_1' w'}$ in (A 4), and that this flux is constant over the height of the experimental tank. This will be the case if the first two terms are small compared to $\overline{\rho_1' w'}$. (The possibility that the first two terms cancel may be ruled out since calculations show that the magnitude of the first term is considerably greater than that of the second term.)

Consider the magnitudes of these terms separately. We will denote the first term by $\Delta q_1(\bar{\rho}_1)$; it is of the order of

$$\Delta q_1(\bar{\rho}_1) = \frac{1}{T}\left\{\int_0^H \bar{\rho}_1(z,T)\,dz - \int_0^H \bar{\rho}_1(z,0)\,dz\right\}. \tag{A 5}$$

For experiments with high values of Ri^*, ($\geqslant 20$) the measured salt flux is small, and the accuracy in measuring the density is important. For example, the amount of salt added during the whole course of this type of experiment may be such that it would cause a density change of $0{\cdot}001\ \mathrm{g\ cm^{-3}}$ if it were added to the total volume of salt water in the system. As the density measurement may be in error by $\pm 0{\cdot}0001\ \mathrm{g\ cm^{-3}}$, the actual flux could be that causing a density change of $0{\cdot}001 \pm 0{\cdot}0001\ \mathrm{g\ cm^{-3}}$ and so there may be a $\pm 10\,\%$ error in our measured flux. Using this error in measurement to represent the variation in density in (A 5), the values of $\Delta q_1(\bar{\rho}_1)$ for various experiments have been calculated and, after multiplication by g/ρ_0, are listed as the buoyancy fluxes $\Delta q(\bar{\rho})$ in table 2. As can be seen, these unsteady components vary from approximately 2–15 % of the measured values of q also listed in this table.

The magnitude of the second term in (A 4) has been calculated over the height of the tank. At $z = 0$ we use the mean velocity that is caused by the addition of salt to the storage system. This velocity would be constant over the height of the experimental tank if the density of the fluid in the tank were homogeneous. But, between the two homogeneous layers, there is a region with a strong density gradient and the diffusion which occurs here can cause a mean vertical velocity to exist at the interface. This can be seen by considering the diffusion equation,

$$\nabla . \mathbf{u} = (K/\rho_0)\nabla^2 \rho_1, \tag{A 6}$$

where we have used both the Boussinesq approximation and the continuity equation. Let ds/dt represent the volume rate at which salt is added to the system and integrate (A 6) over the complete volume of salt-water fluid in the system. The only surfaces through which fluid flow can occur are S_1, the free surface in the salt-water storage tank, and S_2, the salt-water–fresh-water interfacial surface. We will regard S_1 as an impervious surface, kept at a fixed height except for the

volume flow, at the rate ds/dt, through it. The surface S_2 coincides with the region of maximum density gradient in the flow tank. Integration of (A 6) yields

$$\int_{V_s} \nabla . \mathbf{u}\, dv = \frac{K}{\rho_0} \int_{V_s} \nabla . \nabla \rho_1 dv, \tag{A 7}$$

where V_s is the total volume of salt water. Use of the divergence theorem gives

$$\int_{S_1} \mathbf{u} . \mathbf{n} dS_1 + \int_{S_2} \mathbf{u} . \mathbf{n} dS_2 = \frac{K}{\rho_0} \int_{S_2} \mathbf{n} \cdot \nabla \rho_1 dS_2, \tag{A 8}$$

that is,

$$-\frac{ds}{dt} + \overline{w} A = \frac{AK}{\rho_0} \left(\frac{\partial \overline{\rho}_1}{\partial z} \right)_{S_2} \tag{A 9}$$

or

$$\overline{w} = \frac{1}{A} \frac{ds}{dt} - \frac{K}{\rho_0} \left| \frac{\partial \overline{\rho}_1}{\partial z} \right|_{S_2} . \tag{A 10}$$

The value of the first term on the right-hand side of (A 10) is that due to adding salt. For example, 35·8 g added to storage causes an additional volume of approximately 12 cm^3 to be added to the system over a 10 min period. When divided by the horizontal area of the experimental tank and by time, this gives a contribution $\overline{w} \simeq 2 \times 10^{-5}$ cm sec^{-1}. The magnitude of the second term of the right-hand side of (A 10) has been calculated using the maximum density gradient which occurred at the interface during any experiment. This gives a contribution to $\overline{w}$ typically of the order of 10^{-8} cm sec^{-1} and as such is completely negligible. The associated values of $\overline{w\rho}$ were negligible compared to q and are omitted from table 2.

REFERENCES

Axford, D. N. 1968 On the accuracy of wind measurements using an inertial platform in an aircraft, and an example of the vertical mesostructure of the atmosphere. *J. Appl. Meteor.* **7**, 645.

Batchelor, G. K. 1953 *The Theory of Homogeneous Turbulence.* Cambridge University Press.

Clutter, D. W. & Smith, A. M. O. 1961 Flow visualization by electrolysis of water. *Aerospace Engng.* **20**, 24.

Cooper, L. H. N. 1967 Stratification in the deep ocean. *Sci. Prog.* **55**, 73.

Ellison, T. H. & Turner, J. S. 1959 Turbulent entrainment in stratified flows. *J. Fluid Mech.* **6**, 423.

Kato, H. & Phillips, O. M. 1969 On the penetration of a turbulent layer into a stratified fluid. *J. Fluid Mech.* **37**, 643.

Lofquist, K. 1960 Flow and stress near an interface between stratified liquids. *Phys. Fluids*, **3**, 158.

Ludlam, F. H. 1967 Characteristics of billow clouds and their relation to clear-air turbulence. *Q. J. Roy. Meteor. Soc.* **93**, 419.

Long, R. R. 1970 A theory of turbulence in stratified fluids. *J. Fluid Mech.* **42**, 349.

Odell, G. M. & Kovasznay, L. S. G. 1969 A new type of water channel with density stratification. Unpublished manuscript. Department of Mechanics, The Johns Hopkins University.

Reiter, E. 1969 The nature of clear-air turbulence. *Clear-Air Turbulence and its Detection.* New York: Plenum.

Rouse, H. & Dodu, J. 1955 Diffusion turbulente à travers une discontinuité de densité. *La Houille Blanche*, **10**, 522.

TOWNSEND, A. A. 1956 *The Structure of Turbulent Shear Flow*. Cambridge University Press.

TOWNSEND, A. A. 1958 Turbulent flow in a stably stratified atmosphere. *J. Fluid Mech.* **3**, 361.

TURNER, J. S. 1968 The influence of molecular diffusivity on turbulent entrainment across a density interface. *J. Fluid Mech.* **33**, 639.

WOODS, J. D. 1968 Wave induced shear instability in the summer thermocline. *J. Fluid Mech.* **32**, 791.

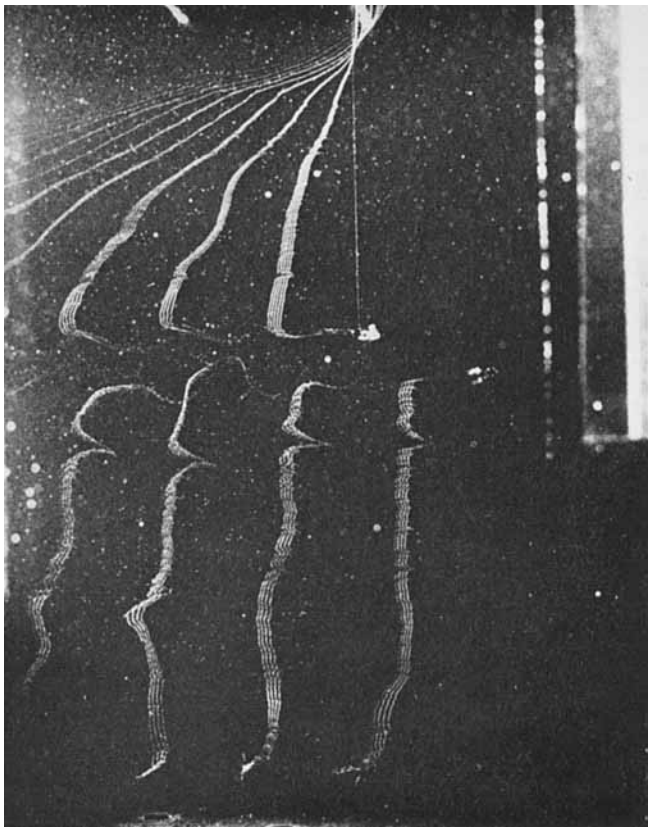

FIGURE 6. Photograph of velocity profile at low value of $Ri^*(\simeq 2)$. Print has been enlarged to show detail illustrated by bubble 'time lines' which are approximately 2 cm apart. The lower half of the channel is shown with the layer of zero velocity near the top of the photograph.

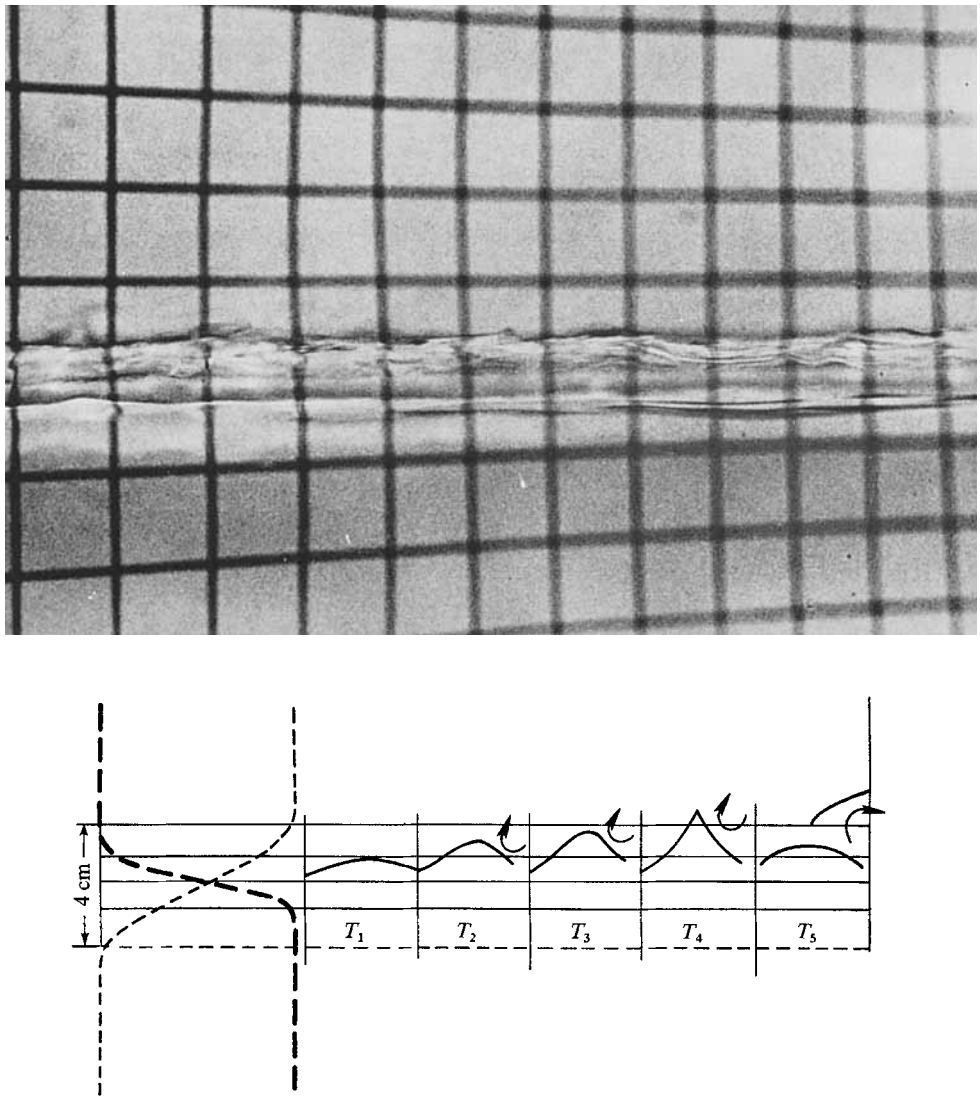

FIGURE 7. Photograph is interface (from slightly above it) at $Ri^* = 15$. Background grid is 2 cm by 2 cm. Sketch is of the development of the undulations seen in the upper photograph and the transfer mechanism which occurs at high values of Ri^*. The velocity profile is linear over 4 cm while most of the density change occurs over 2 cm. – – –, velocity $\Delta u = 4$ cm sec^{-1}; - -, buoyancy $\Delta\rho = 32$ cm sec^{-2}.

FIGURE 8. Wave breaking and roller formation at low values of $Ri^*(\simeq 2)$. The density inflexion point is about 3 cm from the bottom of the picture. Note the eddies from breaking waves which have penetrated into the region of maximum density gradient and the disturbances along the top of this region. Background grid is 2 cm by 2 cm.